RSC Advances

ROYAL SOCIETY OF CHEMISTRY

www.rsc.org/advances

RCS Advances

ARTICLE

Forced Infiltration of Silica beads into Densely-Packed Glass Fibre Beds for Thin Composite Laminates

Received 00th January 20xx,
Accepted 00th January 20xx

DOI: 10.1039/x0xx00000x

www.rsc.org/

Ye Chan Kim[a], Hyunsung Min[d], Jeongsu Yu[d], Sung Yong Hong[b], Mei Wang[a], Sang Hoon Kim[a], Jonghwan Suhr[a,b], Young Kwan Lee[c], Kwang J Kim[e], and Jae-Do Nam*[a,b]

Along with the advancement of miniaturized mobile devices, the packaging technology requires utmost high performance of the thin composite laminates in terms of such materials properties as coefficient of thermal expansion (CTE) and stiffness. These two properties have been improved by incorporating the secondary fillers (e.g., nano-sized silica beads) into the densely-packed glass fibre beds in the composite laminates. However, the secondary fillers are hardly impregnated but usually filtered out by the fibrous bed giving poor distribution of fillers. In this study, we used ultrasonication at a specific range of frequency and time to induce the bubble implosion and its microjetting, which could repulse the adjacent fibres desirably creating the interstitial space for the secondary filler particles to move into through the densely-packed fibrous bed. The migrated secondary fillers facilitated the stress transfer among the beads and fibres, and subsequently altered the thermo-mechanical properties to a great extent. More specifically, the coefficient of thermal expansion (CTE) was greatly decreased by the ultrasonication from 9.8 ppm/K to 6.1 ppm/K by 38% at 25°C, and from 20.6 ppm/K to 15.8 ppm/K about 23% at 175°C. The storage modulus was increased from 7.3 GPa to 9.0 GPa by 23% at 40°C. There achievements are thought to be critical improvements in the development of high performance micropackaging devices. Anisotropic ultrasonication was demonstrated to be utilized as a driving force for the cooperative distribution of thermo-mechanical stresses through the bulk movement of densely-packed fibres and nanoparticles.

Introduction

As the mobile devices are miniaturized more and more in smart phones, tablet PCs, and wearable devices, etc., high density packaging technologies are used to reduce the assembly area of substrates. The package-on-package (PoP) technology, which is one of the most advanced three-dimensional packaging technologies, has been massively adopted particularly for smaller and thinner systems. In this packaging method, the top memory package is integrated on the bottom application processor (AP) one to reduce the occupying space as much as possible, using the most advanced materials and processing technology. The PoP fabrication is carried out by using very thin (ca. 40 μm) and stiff (Young's modulus at 15 GPa) glass fibre/epoxy composite laminates often containing over 60 vol% of silica fillers without void defects. The PoP construction requires the welding assembly process, which accompanies repeated thermal cycles at elevated temperatures usually up to 260°C. These thermal curing/welding processes generate mismatched thermal expansion of different materials of epoxy-based polymers, metal electrodes, and semiconductor chips, which subsequently creates substantial amount of thermal stresses. The coefficient of thermal expansion (CTE) of the semiconductor AP chip, which is made from silicon, is ca. 3 ppm/K, which should be compared with 16.5 ppm/K of copper, 54 ppm/K of epoxy, and 18–20 ppm/K of its glass fibre composite. Consequently, these CTE mismatch and thermal stresses thereof often give serious failures of the printed circuit boards (PCB) appearing as warpage of assembled PCB parts, connection failure, long-term durability, etc. Accordingly, one of the key issues in advanced packaging technology is currently the development of low-CTE polymer-based composite laminates.

In addition to those thermal stresses, the UV/thermal curing of epoxy/glass-fibre prepregs, photoresists, and adhesives repeatedly provide a large amount of volumetric shrinkage due to the liquid-to-solid phase transformation of curing, which may very well give rise to internal stresses. These thermal and curing-induced stresses should be overcome by the robustness of the PCB frame structure, that is, the

[a] Department of Energy Science, Sungkyunkwan University, 2066, Seobu-ro, Jangan-gu, Suwon-si, Gyeonggi-do, Republic of Korea
[b] Department of Polymer Science and Engineering, Sungkyunkwan University, 2066, Seobu-ro, Jangan-gu, Suwon-si, Gyeonggi-do, Republic of Korea
[c] Department of Chemical Engineering, Sungkyunkwan University, 2066, Seobu-ro, Jangan-gu, Suwon-si, Gyeonggi-do, Republic of Korea
[d] Information Technology & Electronic Materials Research Institute, LG Chem, Ltd. Research Park, 104-1, Moonji-dong, Yuseong-gu, Daejeon, Republic of Korea
[e] Department of Mechanical Engineering, University of Nevada Las Vegas, 4505 S. Maryland Parkway, Box 454027, Las Vegas, NV 89154-4027, USA
*Email: Prof. J.-D. Nam jdnam@skku.edu
Electronic Supplementary Information (ESI) available: [details of any supplementary information available should be included here]. See DOI: 10.1039/x0xx00000x

imbedded sheet of epoxy/glass fibre composite laminates. For example, a typical 'flip chip chip scale package' (FCCSP), which is recently applied to mobile AP, is often composed of 4 printed circuit layers in the thickness of 600 μm, of which the stiffness should be sustained by only 2–3 layers of epoxy/glass composite laminates, each ca. 40 μm in thickness. Therefore, it is desperately needed to increase the modulus of the composite laminates while having low CTE values and loading contents. It may be achieved using the primary fibre fabric and the secondary silica bead that can maximize the interfacial area (or work of adhesion) of reinforcing fillers.[1, 2]

Currently, the most advanced ultra-thin prepreg is extremely highly loaded with reinforcing fillers. One of the commercialized prepreg systems is, for example, composed of the stiffest glass fibre, T-glass fibre (20–25 wt%) as a main skeletal frame structure and tremendous amount of silica beads (60–70 wt%) as a secondary filler. Only 15–20 wt% of epoxy matrix material is used. This type of composite laminate is specifically designed to minimize the CTE and simultaneously maximize the stiffness. It also provides excellent interfacial boning and structural integrity with copper as well as silicon in such hostile thermal- and stress-conditions. In such highly loaded secondary filler systems, however, it should be mentioned that it is extremely difficult to achieve even distribution of the secondary beads in the densely-packed skeletal fibre structure of the fibre.

The fabrication of composite structures composed of two different sizes and different forms of shape is usually a challenge. It is difficult to force the secondary fillers to be incorporated in the primary skeletal structure particularly when the bed is densely packed leaving little interstitial space. When the secondary fillers approach a densely-packed structure in composite fabrication, a high shear stress is developed near the interfaces of the two fillers, and subsequently the densely-packed fibres filter the secondary fillers leaving them outside of the primary fibre bed. Therefore, penetration or impregnation of the secondary fillers into the fibre bed can be hardly achieved in such methods as hand lay-up or solvent impregnation processes.[3] As a result, the secondary fillers filtered out by the fibres may very well give poor distribution of thermo-mechanical stresses leading to substantial deterioration of the ultimate performance of the composites structures.[4, 5]

The effect of the spatial distribution of fillers on the effective composite properties has drawn the attention of a number of researchers.[4-9] It has been found that the spatial distribution of reinforcing fillers affects the stress-strain relation at the interfaces of reinforcement and matrix, which could substantially influence the thermo-mechanical properties of the composites.[4-9] Compared with a composite material containing coagulated fillers, an even distribution of reinforcing fillers significantly increase the interface areas of fillers and matrix, where the stresses are transferred, and subsequently increase the thermo-mechanical properties such as tensile strength and elongation.[10, 11] Particularly in our highly-loaded silica bead and anisotropic fibre systems, they could lead to very complicated distribution of stresses. The anisotropic woven glass fabric and heterogeneous filler distribution could result in convex or concave bending, say, "smile" or "cry" warpage in the assembled PCB stacks. These warpage or bending failure caused by a slight imbalance of internal stresses. Thus, a homogenous distribution of silica beads is a significant and critical issue in the fabrication process of prepregs as well as in the final performance of high performance PCBs.

The ultrasonication has been utilized to clean the contaminated surfaces.[12-14] It is also used to disperse such fillers as titanium dioxide nanoparticles, nanoclay, and silica nanoparticles in polymers.[15-18] When a liquid is ultrasonicated, the sound waves propagate through media with an alternate pressure giving compression and rarefaction cycles at a given frequency.[19] During rarefaction, ultrasonic waves create small vacuum bubbles or voids in the liquid, which is called acoustic cavitation. Both ultrasonic cleaning and ultrasonic dispersion use this collapsing energy of the cavitation bubbles to break the cluster of contaminant and/or nanoparticles. It is thought that the bubble cavity, which is repeatedly created and collapsed in every 10^{-6}–10^{-4} sec, may be used to make space among the adjacent fibres or beads desirably for them to be commingled during composite fabrication.[20] Particularly, the nanoparticles may very well move along with the instantaneous fluid flow created by the bubble collapse probably in the direction to the space where the population of nanoparticles is low. We consider that this phenomenon may spatially redistribute two different types of filler systems, forcing the nanosized silica beads into the densely-packed fibre bed in the case of our study.

In this study, we investigated the ultrasonication-assisted secondary filler infiltration into primary skeletal structure and the CTE of the fabricated composite laminates using the epoxy/glass fibre/bead composites as a model system. It was found that the ultrasonication, which was induced during fabrication of composite laminates, led to the even distribution of the secondary filler in the densely-packed fibre bed. The CTE of the composite laminates was significantly decreased by the well-distributed secondary fillers, which seemed to indicate that the stress was transferred in a facile manner between the filler and the matrix. The ultrasonication could be used for the development of highly-loaded multiple-filler composite systems, which improve the efficiency of reinforcement without increasing loading contents by achieving the even distribution.

Experimental

Materials. The main text of the article should appear here with headings as appropriate. T-glass woven fabric, silica beads, and epoxy thermosetting resins were used to fabricate prepregs and

composite laminates. The glass fabric used herein was a T-glass woven fabric with 0.025 mm thickness, 24 g/m^2 weight and 5 µm fibre diameter (T-1039, Nitto Boseki Ltd) (Figure1A and 1B). Silica beads in the diameter range of 50 nm to 1.5 µm with mean particle size of 300 nm were used (SFP-30MHE, DENKA) (Figure 1C and 1D). Silica beads (60 wt%) were incorporated to epoxy resin dissolved in dimethylformamide (DMF), which was supplied by LG Chem Ltd. The epoxy resin solution including the silica beads, which its density was about 1.52 g/cm^3, were mixed until the viscosity reached 50 cps.

Preparation of silica bead incorporated epoxy/glass fibre prepreg and laminates. Prepregs were prepared using a solvent impregnation process at room temperature and ambient humidity, as schematically illustrated in Figure S1 in Supporting Information. The silica beads/epoxy resin solution was mechanically stirred for about 2 h at room temperature. The glass woven fabric was immersed in the silica beads/epoxy resin solution for 120 sec at room temperature, and was then squeezed by squeezing rollers. The prepreg was dried at 160°C in a convection oven for 120 sec to remove the remaining solvent. The final resin content was controlled between 15 – 20 wt%.

The ultrasonicated prepregs were prepared following the above procedure except the impregnation step. Herein, the glass woven fabric was immersed into a mixture solution of silica beads and epoxy resin. The mixture solution contains silica beads (60–70 wt%), epoxy matrices (15–20 wt%), and DMF as a solvent. The ultrasound (400 W / 40 kHz) was applied during the solvent impregnation process using a standing wave ultrasonic bath. The ultrasonication time varied for 10 sec and 120 sec in this study for comparison.

The prepregs were cut to the size of 130 mm wide and 150 mm long. And then they were cured under a controlled temperature program, where the temperature increased up to 225°C at 2 K/min under the pressure of 5 MPa, and then held for 75 min to make the composite laminates. The density of the fully cured laminates was about 1.89 g/cm^3.

Characterization. Scanning electron microscope (SEM) images of silica beads and the glass woven fabric were obtained by using a JEOL JSM-7401F. The composite laminate samples obtained with different ultrasonication times (0, 10, and 120 sec) were investigated using an optical microscope (Nikon ECLIPSE 80i) and the scanning electron microscope (JEOL JSM-7401F). The composite laminate samples embedded in epoxy resin were polished to investigate the cross section of the composite laminates. The in-plain direction thermal expansion coefficient of composites was measured with the Seiko Exstar 6000 (TMA6100) thermal mechanical analyzer (TMA) under the heating rate of 5°C/min up to 300°C in air. The TMA samples, which are fully cured composite laminates, were prepared as the size of 3 mm wide, 30 mm long, and about 40 µm thick. Dynamic mechanical analysis (DMA) was carried out in tension mode using the Seiko Exstar 6000 (DMA/SS6100) at a frequency of 1 Hz with a 10 µm amplitude under the heating rate of 3°C/min up to 300°C. The DMA samples, which are fully cured composite laminates, were prepared as the size of 5 mm wide, 40 mm long, and about 40 µm thick. Thermogravimetric analysis (TGA, TA instruments Q50) was conducted in a nitrogen atmosphere from ambient temperature to 750°C with heating rate of 10°C/min.

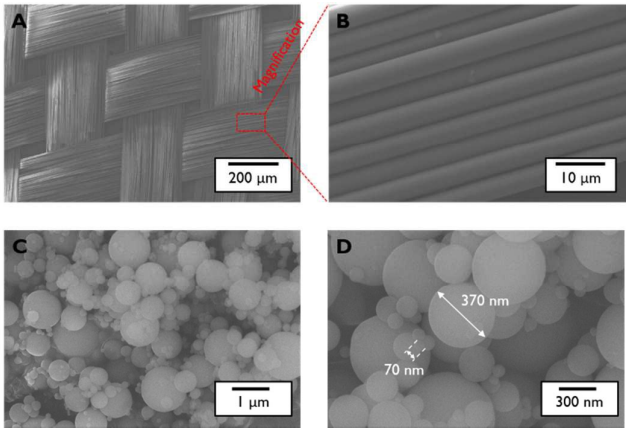

Figure 1. SEM images of glass fibre woven fabric (A), densely-packed glass fibre bed with mean glass fibre diameter of 5 µm (B), and size distribution of silica beads used as secondary filler in this study with mean particle size of 500 nm at different magnification (C) and (D)

Results and Discussion

Isotropic bubble collapse and anisotropic cavitation microjet. As mentioned previously, due to the abrupt collapse of the cavitation bubble (Figure 2A), huge energy is concentrated in the bubble and the temperature increased rapidly, because the heat has no time to escape from the bubble, which complies with almost the adiabatic process. Theoretically, the temperature increases up to 5000 K and the pressure reaches about 1000 atm. Consequently, this interesting phenomena associated with such concentrated energy generates either shock wave or microjet each corresponding to isotropic and anisotropic collapse of bubbles as seen in Figure 2A, and 2B, respectively.[21-23] The shock waves and bubbles may well push away adjacent fibres to make space for the secondary nano-sized fillers to migrate inside.

In the theory of ultrasonic cavitation, when the solid wall is several times larger than the resonance bubble, e.g. bigger than 200 µm at 20 kHz in water [24, 25], the anisotropic microjet is created from a solid wall while the potential energy of the expanded bubble is converted into kinetic energy near the solid wall. In this study, it may very well think that the densely-packed woven glass fabric acts as a solid wall. When the ultrasound applied to the matrix liquid in the presence of the glass fabric, the anisotropic microjet occurs near the tightly packed glass fibres (Figure 2B), which is very

different from the isotropic formation of isolated bubbles (Figure 2A). When a cavitation bubble is produced near a solid interface, an asymmetric deformation of the cavity occurs to give an asymmetric liquid motion during cavity collapse. This asymmetric cavity deformation results in a liquid microjet, which may very well carry the nano-sized fillers with the jet to penetrate into the fibrous bed. The collapse of an asymmetric cavitation bubble is described by Bernoulli's equation, restating the pressure on the free surface in terms of the velocity potential (φ) and the velocity of the fluid (v),

$$\frac{\partial \phi}{\partial t} + \frac{1}{2} v^2 = \frac{\Delta p}{\rho_L}$$

(1)

where Δp is the pressure difference between the ambient liquid pressure and the vapour pressure, and ρ_L is the density of the fluid.

In this equation, it can be assumed that the normal derivative of velocity potential must vanish at the solid interface, and the initial potential is uniformly zero.[26] Then, the speed of the microjet, U_J at the time it impacts the opposite surface of the bubble may be derived as

$$U_J = \xi (\Delta p / \rho_L)^{1/2}$$

(2)

impacts the opposite surface of the bubble may be derived as where ξ is a constant. The collapse of the distorted bubble generates a high-speed microjet. It reaches the maximum jet speed of 110–140 ms^{-1} with theoretical calculations at atmospheric pressure, room temperature, and the density of 1.52 g/cm^3, which seems to give sufficient impact power to the solid/liquid interfaces and subsequently expand the interstitial space between the beads and fibers.[27]

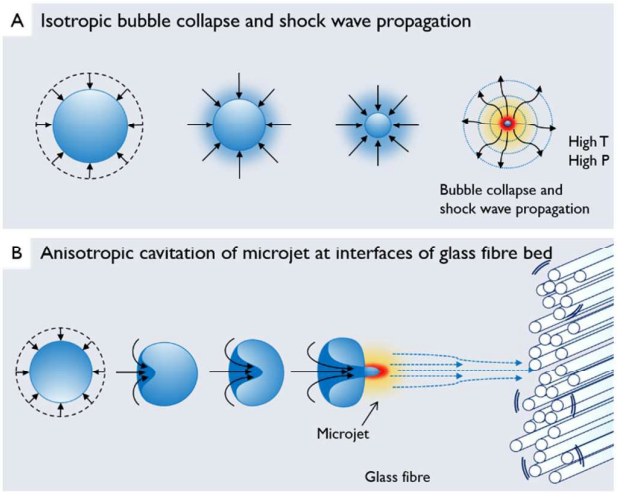

Figure 2. Isotropic bubble collapse (A) generating isotropic shock waves resulting in radial wave propagation facilitating bead dispersion and fibre spreading. Anisotropic bubble collapse near solid interface boundaries (B) generating high-speed microjet delivering the beads into the spread glass fibre bed

Secondary filler infiltration by ultrasonic bubble implosion and anisotropic microjet. Figure 3 shows the ultrasonication-assisted migration process, where the secondary silica beads moves into the primary fibre bed during solvent impregnation process. When the primary fibre bed is simply immersed in the secondary-filler mixture solution, the silica beads can hardly infiltrate into the glass-fibre bed (Figure 3A). When the ultrasound energy is applied and generates cavitation bubbles in the mixture, the implosion of bubbles in the fibre bed generates shock wave that radially propagates to push the adjacent packed fibres away (upper part of Figure 3B). In addition, the high-speed anisotropic microjet is derived by the boundary interfaces, which provides nonspherical implosion of the cavitation bubble in an anisotropic way into the primary fibrous filler interfaces (lower part of Figure 3B). This microjet may carry the secondary beads to move inside the interstitial space of fibre bed; subsequently, the secondary beads migrate along with the sonication induced resin flow. These two isotropic and anisotropic bubble implosion may very well allow the secondary fillers to move into the primary fibrous filler bed (Figure 3C). Finally, Figure 3D shows the stabilized feature where the secondary beads are well distributed inside the fibre beds, which should be compared with the segregated feature of the primary and secondary fillers in Figure 3A.

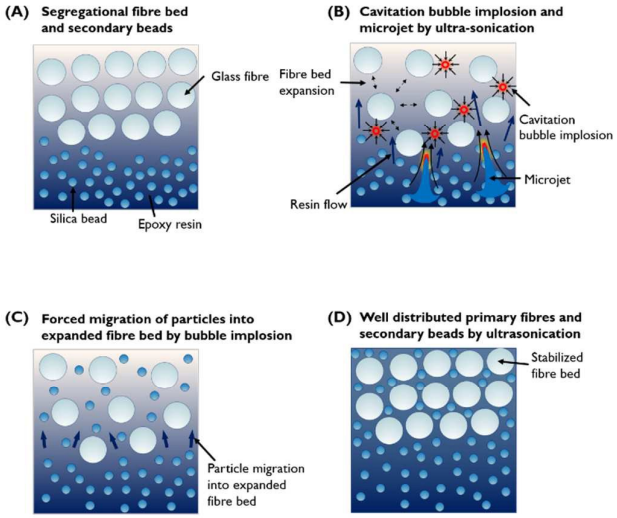

Figure 3. Schematic of migration of secondary filler of beads into primary fibre bed during solvent impregnation process. The secondary beads is filtered out and segregated by the fibre bed (A). When ultrasonication induced, densely-packed fibre bed are expanded by the implosion of the cavitation bubbles in the fibre bed which generates shock wave. The secondary beads are injected and migrated along with the high-speed anisotropic microjet, which is derived by the boundary interfaces of fibres (B, C). As a result, the secondary beads are well distributed inside the fibre bed (D). The sizes of the cavitation bubble implosion and the microjet are not realistic. In cavitation theory, the theoretical radius of the resonance bubble is 0.1–110 μm at 20 KHz in water.

Experimental observation of silica beads and glass fibre composite comparing ultrasonication effects. Figure 4 shows the cross section of a typical composite laminate prepared without applying ultrasonication. As can be seen, a densely-packed glass fibre woven fabric sheet is shown at the centre (about the thickness of 25 μm), and the resin solution/silica bead mixture is impregnated from left and right sides. When there is no ultrasonication, the silica beads are filtered and thus observed on both sides of glass fabric appearing as small grey dots in the figure. It is believed that the woven fabric is usually so densely-packed that the silica beads can hardly penetrate into the fabric. Thus, there appears the resin-rich region inside the densely-packed woven fabric as clearly indicated in Figure 4. It is evident that the facile migration or even distribution of silica beads can hardly be achieved without the assistance of ultrasonication due to the filtering effect of the densely-packed fibre bed.

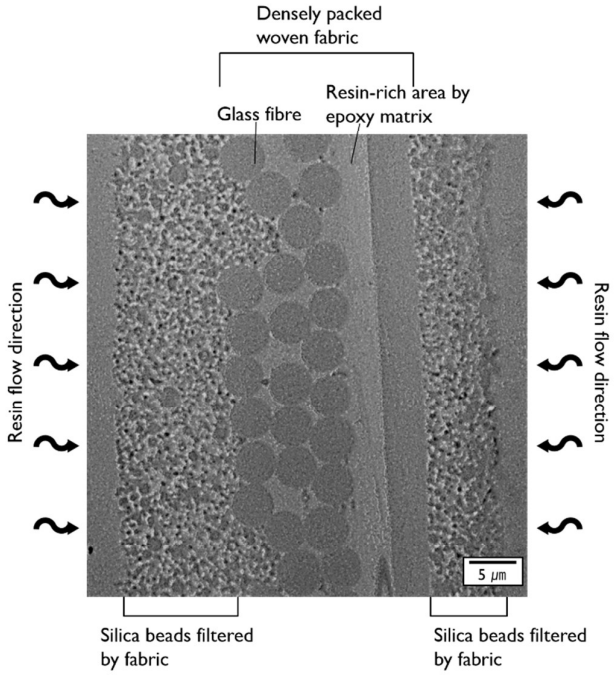

Figure 4. Optical micrographs image of epoxy/glass fibre/bead composite specimen (cross-sectional image) without ultrasonication, illustrating the filtering of silica beads by densely-spaced fibres

Morphology change of epoxy/glass fibre/bead composite laminates by ultrasonication. When ultrasonication is applied, the forced infiltration of silica beads into densely-packed glass fibre bed is clearly seen in Figure 5. It compares the epoxy/glass fibre/bead composite laminate specimens prepared without sonication (A), with 10 sec sonication (B), and with 120 sec sonication (C). Figure 5A (the full image of Figure 4) illustrates the case that no sonication is applied, clearly showing the segregated silica beads accumulated on both left and right outsides of the specimen. It looks clear that the silica beads are filtered out by the glass fibre bed. Figure 5B illustrates the case that the sonication is applied relatively for a short period of time (10 sec in this study). It shows that the small amounts of silica beads are impregnated into the glass fibre bed. The figure demonstrates that the infiltration of the silica beads into the glass fibre bed due to the shock wave and anisotropic microjet, as mentioned earlier. Figure 5C illustrates the case that the sonication time is further increased to 120 sec, showing that the glass fibre bed is completely filled with the silica beads. It is likely that the sonication distributes the silica beads without changing the loading contents of them in composites laminates (Figure S2 in Supporting Information). Figure S2 shows the similar residual weight which is the weight of fillers for the three laminate specimens. It should be mentioned that it can hardly be achieved without ultrasonication by simply extending the impregnation time or using typical roll-to-roll pressing in the prepreging processes. It is believed that the controlled ultrasonication can facilitate the impregnation of secondary fillers into densely-packed fibre beds in

an effective way that cannot be achieved by other conventional processing techniques.

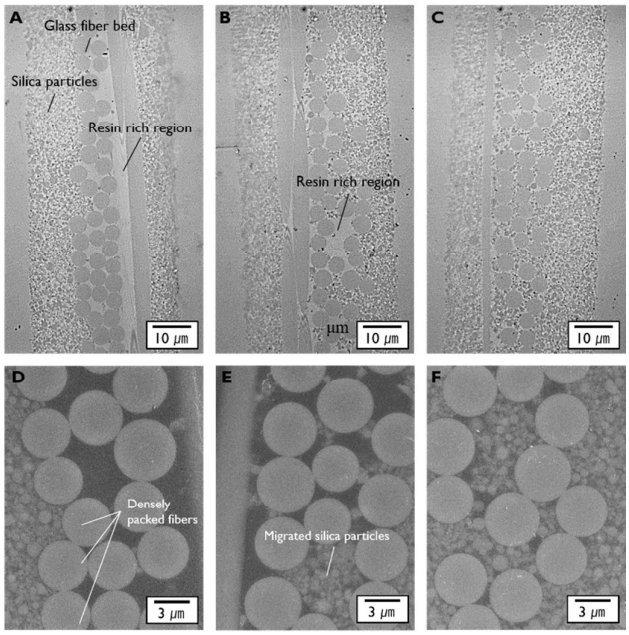

Figure 5. Optical micrographs and SEM images of silica bead incorporated of epoxy/glass fibre composite laminate specimens (cross-sectional images), illustrating the migration of the silica beads on the glass fibre bed at different ultrasonication time: w/o sonication (A, D), with 10 seconds sonication (B, E), and with 120 seconds sonication (C, F)

Coefficient of thermal expansion (CTE) of epoxy/glass fibre/bead composite laminates. Figure 6 compares the thermal strain of our composite laminate specimens in the in-plane principal direction plotted as a function of temperature, comparing three specimens as used for the analysis of Figure 5, each corresponding to the sonication times at 0, 10, and 120 sec, respectively. Figure 6 shows the same glass transition temperature (T_g) at 175°C for three composite laminate specimens. The slope of the specimen dimension represents the CTE. In two regions, below T_g and above T_g, the three laminate samples give different slopes (or CTEs). The CTEs are likely to decrease as the ultrasonication time increases.

From the linear region of slopes between 80 – 160°C (below T_g) and 180 – 260°C (above T_g), the CTEs of the laminate specimens were obtained, and subsequently plotted as a function of temperature in Figure 7. It is clear that the CTEs increase with temperature in a linear fashion in the whole region of temperature. Accordingly, the CTEs may be fitted by the following equation.

$$\alpha = \alpha_0 + \beta(T - T_{ref}) \quad (3)$$

where α_0 is the coefficient of thermal expansion at reference temperature, β is the gradient, and T_{ref} is the reference temperature. The reference temperatures are taken as 25°C for below T_g and 175°C for above T_g for all the three specimens. The α_0 and β values for two regions below- and above-T_g are summarized in Table 1. Comparing the specimens with 120 sec sonication and w/o sonication, the α_0 value below-T_g is 6.1 ppm/K which is 38% lower than the α_0 value of the specimen w/o sonication (9.8 ppm/K). The α_0 value above-T_g is 15.8 ppm/K, also present 23% lower value than the α_0 value of the specimen w/o sonication (20.6 ppm/K). The β values of three specimens below-T_g are similar at 0.023 – 0.025. The β values of the specimens with 10 sec sonication and w/o sonication above-T_g are decreased to 0.014 and 0.013, while β values of the specimens with 120 sec sonication above-T_g remains stationary.

It is clear that the even distribution of silica beads significantly changes the CTE of the composite laminates. In the below-Tg region, the CTE ranges 10.5–13.2 ppm/K for the w/o ultrasonication and 6.9–8.5 ppm/K for w/ ultrasonication. The even distribution of silica beads influences the local stress distribution, which subsequently affects the effective properties of the composite such as thermal expansion stress, fatigue, and tensile strength.[6, 8, 9] Especially, at high loading contents of fillers, the effect of the spatial distribution of particle on the effective properties of composites is increased.[28] With our highly loaded silica beads and glass fibre system, the spatial distribution of two different filler seems to have strong influence on the CTE of the composite laminates. When the silica beads are uniformly distributed via the ultrasonication, as seen in Figure 5C, the silica beads are likely to redistribute silica bead interfaces, which effectively convert the thermal stresses as hoop stresses around the surface of glass fibres and the silica beads. Although the composite systems shown in Figure 5 have the same filler content or the same surface area of filler-exposed surfaces, the apparent CTEs differ to a great extent by up to 38%. This surprising result shows the possibility that the thermo-mechanical properties of the composites are substantially influenced by the spatial distribution of fillers.

This work may propose a solution to the secondary filler filtering issues, which are faced quite often in many occasions fabricating multiple-filler composite systems. Our work clearly demonstrates an efficient way of impregnating secondary fillers in such a densely-packed fibre system without the need of lowering the loading contents of the fillers. Moreover, this investigation can be further extended to the development of different-filler composite systems in different shapes, sizes, packing types, etc.

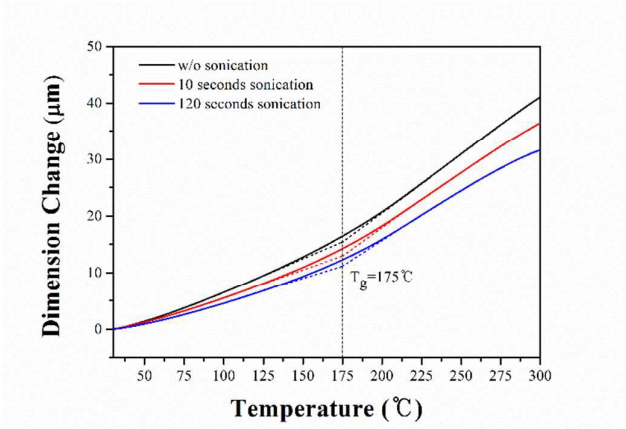

Figure 6. Dimensional change of epoxy/glass fibre/bead composite laminates in the in-plane direction comparing three cases: w/o sonication, 10 seconds sonication, and 120 seconds sonication as a function of temperature.

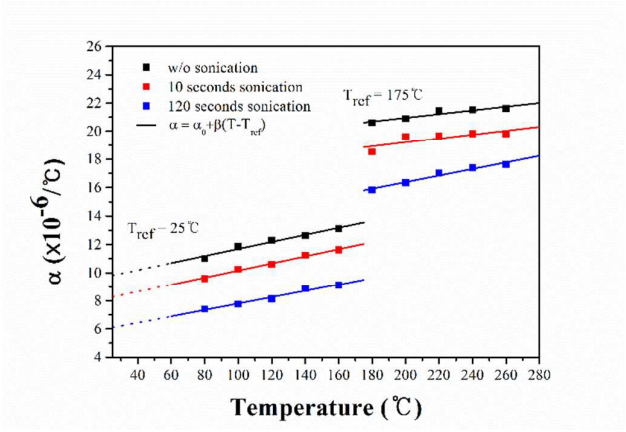

Figure 7. The CTE of epoxy/glass fibre/bead composite laminates w/o sonication, 10 sec sonication, and 120 sec sonication, compared with the model equation, ($\alpha = \alpha_0 + \beta (T - T_{ref})$)

Table 1. The parameters (α0 and β) of the CTE model equation ($\alpha = \alpha_0 + \beta (T - T_{ref})$) for both below and above the glass transition temperature (T_g)

	Below T_g (T_{ref} = 25°C)		Above T_g (T_{ref} = 175°C)	
	α_0 (ppm/K)	β	α_0 (ppm/K)	β
w/o sonication	9.8	0.025	20.6	0.013
10 sec sonication	8.3	0.025	18.8	0.014
120 sec sonication	6.1	0.023	15.8	0.023

Dynamic mechanical analysis (DMA) of epoxy/glass fibre/bead composite laminates. The DMA results for all the specimens are plotted in Figure 8, which shows variation of storage modulus E', loss modulus E'', and tan δ as a function of temperature and Cole-Cole plot of storage and loss moduli. The storage modulus E' and loss modulus E'' (Figure 8A and 8B), respectively, represents the ability of materials to resist elastic and viscous deformation. Both storage and loss modulus are likely to increase as the ultrasonication time increases in the overall range of temperature. Storage modulus of the specimen w/ 120 sec sonication is 9.0 GPa at 40°C which is 23% higher than that of the specimen w/o sonication (7.3 GPa). The difference between two specimens is gradually decrease as temperature increased. Loss modulus of the specimen w/ 120 sec sonication is 345 MPa at 40°C which is 38% higher than that of the specimen w/o sonication (236 MPa). The difference between two specimens is much higher (46%) at the peak where the temperature is 260°C. Figure 8C shows damping coefficient (or tan δ) of three specimens; w/o sonication, 10 sec sonication, and 120 sec sonication, having the same peak (T_g) at 270°C reaching 0.045, 0.051, and 0.056, respectively. Figure 8D presents Cole-Cole plot of storage and loss moduli of three specimens. They show a parabolic shape in the modulus range of the glass transition. The plots show parallel translation to diagonal direction as sonication time increased. It is considered that the spatial distribution of two different fillers highly affects both stiffness and damping behaviour of composite laminates, which shows good agreement with the TMA results.

It is well known that T_g is dependent on the thermal analysis techniques and the glass transition is a relaxation phenomenon usually taking place in a range of temperature. In this study, T_g obtained from DMA is usually measured higher than that of TMA, and DMA signals respond more sensitively to the reinforcing materials, which usually give increased T_g.[29] In Figure 8B, the loss modulus of three specimens shows a broad range of T_g transition representing the onset point at around 150°C, which seems to correspond to the T_g of TMA. The mechanical onset points of DMA are seemingly induced from a slight rearrangement of woven glass fabric stemming from the matrix softening, which seems to correspond to the volumetric changes detected by TMA.

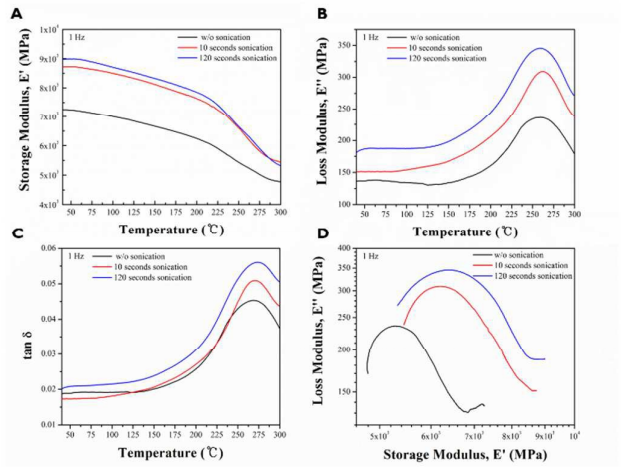

Figure 8. Thermo-mechanical properties of epoxy/glass fibre/bead composite laminates w/o sonication, 10 sec sonication, and 120 sec sonication obtained from DMA tests at 1 Hz. (A) storage modulus E', (B) loss modulus E'', (C) tan δ , and (D) Cole-Cole plot of E' and E''.

Conclusions

We investigated the forced infiltration of the secondary fillers into the primary skeletal structure and the CTE of the fabricated composite laminates in highly-loaded multiple-filler composite systems. The secondary filler, silica bead, was infiltrated into the primary skeletal structure, the densely-packed glass fibre bed, by the shock wave and anisotropic cavitation microjet, which occurs in the glass fibre bed and its interfaces during ultrasonication. The even distribution of silica beads, which was achieved by forced infiltration, was verified by morphological analyses. The maximized stress transfer through evenly distributed two different sized filler significantly reduced the CTE and enhance the stiffness of the composite laminate. It is believed that this investigation could provide an opportunity to effective reinforcing for highly-loaded multiple-filler composite systems.

Acknowledgements

This work was supported by the National Research Foundation of Korea (NRF), the Ministry of Science, ICT & Future Planning (NRF-2012M1A2A2671788 and NRF-2014M3C1B2048175), and Ministry of Trade, Industry and Energy (MOTIE) (10041173). We also appreciated the project and equipment support from Gyeonggi Province through the GRRC program in Sungkyunkwan University. KJK thanks the partial from the US National Science Foundation (#1545875).

Notes and references

1. G. Gao, *Nanostructures and nanomaterials: synthesis, properti es and applications*, London: Imperial College Press, London, 2 004.
2. R. F. Gibson, *Principles of composite material mechanics*, CRC press, Florida, 2011.
3. M. Quaresimin and R. J. Varley, *Composites Science and Technology*, 2008, **68**, 718-726.
4. K. Zhang, L. Wang, F. Wang, G. Wang and Z. Li, *Journal of applied polymer science*, 2004, **91**, 2649-2652.
5. Y. Yang, Z.-k. Zhu, J. Yin, X.-y. Wang and Z.-e. Qi, *Polymer*, 1999, **40**, 4407-4414.
6. J. Sarkar, T. Kutty, K. Conlon, D. Wilkinson, J. Embury and D. Lloyd, *Materials Science and Engineering: A*, 2001, **316**, 52-59.
7. J. Segurado, C. Gonzalez and J. Llorca, *Acta Materialia*, 2003, **51**, 2355-2369.
8. J. Segurado and J. LLorca, *Mechanics of materials*, 2006, **38**, 873-883.
9. M. Chaturvedi and Y.-L. Shen, *Acta materialia*, 1998, **46**, 4287-4302.
10. D. Zhang, K. Sugio, K. Sakai, H. Fukushima and O. Yanagisawa, *Materials transactions*, 2007, **48**, 171-177.
11. Z. d. M. Boari, W. A. Monteiro and C. A. d. J. Miranda, *Materials Research*, 2005, **8**, 99-103.
12. D. Ensminger and F. B. Stulen, *Ultrasonics: data, equations and their practical uses*, CRC press, Florida, 2008.
13. R. N. Weller, J. M. Brady and W. E. Bernier, *Journal of Endodontics*, 1980, **6**, 740-743.
14. E. Maisonhaute, C. Prado, P. C. White and R. G. Compton, *Ultrasonics sonochemistry*, 2002, **9**, 297-303.
15. B. Bittmann, F. Haupert and A. K. Schlarb, *Ultrasonics sonochemistry*, 2009, **16**, 622-628.
16. C.-k. Lam, K.-t. Lau, H.-y. Cheung and H.-y. Ling, *Materials Letters*, 2005, **59**, 1369-1372.
17. M. F. Uddin and C. T. Sun, *Composites Science and Technology*, 2010, **70**, 223-230.
18. C. Braver, M. Tumey, A. Harlow and Q. Han, ASME 2009 International Manufacturing Science and Engineering Conference, Volume 1, West Lafayette, Indiana, USA, October 4–7, 2009.
19. K. S. Suslick, Y. Didenko, M. M. Fang, T. Hyeon, K. J. Kolbeck, W. B. McNamara, M. M. Mdleleni and M. Wong, *Philosophical Transactions of the Royal Society of London. Series A: Mathematical, Physical and Engineering Sciences*, 1999, **357**, 335-353.
20. W. Lauterborn and C.-D. Ohl, *Ultrasonics Sonochemistry*, 1997, **4**, 65-75.
21. K. Suslick and S. Doktycz, *Adv. Sonochem*, 1990, 1, 197-230.
22. K. S. Suslick, *Science*, 1990, **247**, 1439-1445.
23. K. S. Suslick, *Ultrasound: its chemical, physical, and biological effects*, VCH Publishers, Weinheim, 1988.
24. A. Brotchie, F. Grieser and M. Ashokkumar, *Physical review letters*, 2009, **102**, 084302.
25. T. Leighton, *The Acoustic Bubble*, Academic Press, London, 199 4.
26. M. S. Plesset and R. B. Chapman, *Journal of Fluid Mechanics*, 1971, **47**, 283-290.
27. J. R. Blake and D. Gibson, *Annual Review of Fluid Mechanics*, 1987, **19**, 99-123.
28. L. Mishnaevsky Jr, K. Derrien and D. Baptiste, *Composites Science and Technology*, 2004, **64**, 1805-1818.
29. R. J. Seyler, *Assignment of the glass transition*, ASTM International, Philadelphia, 1994.